World Academy of Science, Engineering and Technology
International Journal of Mechanical and Mechatronics Engineering
Vol:5, No:9, 2011

Fluid Flow and Heat Transfer Structures of Oscillating Pipe Flows

Yan Su, Jane H. Davidson and F. A. Kulacki

Abstract**—**The RANS method with Saffman's turbulence model was employed to solve the time-dependent turbulent Navier-Stokes and energy equations for oscillating pipe flows. The method of partial sums of the Fourier series is used to analyze the harmonic velocity and temperature results. The complete structures of the oscillating pipe flows and the averaged Nusselt numbers on the tube wall are provided by numerical simulation over wide ranges of Re_A and Re_R. Present numerical code is validated by comparing the laminar flow results to analytic solutions and turbulence flow results to published experimental data at lower and higher Reynolds numbers respectively. The effects of Re_A and Re_R on the velocity, temperature and Nusselt number distributions have been di scussed. The enhancement of the heat transfer due to oscillating flows has also been presented. By the way of analyzing the overall Nusselt number over wide ranges of the Reynolds number Re and Keulegan-Carpenter number *KC*, the optimal ratio of the tube diameter over the oscillation amplitude is obtained based on the existence of a nearly constant optimal *KC* number. The potential application of the present results in sea water cooling has also been discussed.

Keywords**—**Keulegan-Carpenter number, Nusselt number, Oscillating pipe flows, Reynolds number

I. INTRODUCTION

OCEAN wave energy [1] and sea water cooling [2] have been potential sources as renewable energy with high energy densities [3]. The fluid mechanics and heat transfer of oscillating pipe flows are very important for ocean energy applications [4].

The early studies of oscillating flows were highly concentrated on flow structures [5-9]. The flow was observed to be laminar at low Re_A and become turbulent at high Re_A by Ohmi *et al.* [10]. They demonstrated that for $Re_R > 8$, the critical Reynolds number $(Re_A)_{cr}$ for the onset of transition is independent of Re_R: the value of $(Re_A)_{cr} = 4.00\times10^4$ corresponds to the onset of disturbed laminar flow superimposed with small perturbations, while $(Re_A)_{cr} = 1.51\times10^5$ for the onset of intermittently locally-bursting turbulent flow. Akhavan *et al.* [11] also investigated experimentally the transition of oscillating flows in circular pipes. Hino *et al.* [7] observed that the value of $(Re_A)_{cr}$ increased when $Re_R < 5.12$, because the viscous Stokes layers at the pipe wall become relatively thicker when Re_R decreases and the interaction of the Stokes layers from the wall restricts the viscous diffusion for boundary layer growth. Further decrease in Re_R leads to the limit case of a quasi-steady laminar Poiseuille flow. Conversely, the increase of Re_R to a very large value will lead to the other limit case where the Stokes layer becomes much thinner than the pipe radius. To investigate the flow transition as well as its associated wall shear stress, Blondeaux [12] investigated numerically the oscillating flows in a semi-infinite fluid domain over a flat plate by implementing the Reynolds Averaged Navier-Stokes (RANS) method with Saffman's turbulence model [13, 14]. However, he reported only amplitude but no phase angle information on the oscillatory shear stress. The Lam-Bremhorst form of the low-Reynolds number k-□ turbulence model was chosen for oscillating-flow modeling by [15], while there are still some deficiencies due to the shortcomings of the low-Reynolds number computational model. Also the higher order harmonics are not decomposed from the first order one. Hsu *et al.* [16] demonstrated that Saffman's turbulence model is applicable for unsteady oscillating flows and they also provided a complete account for the oscillatory shear stress on the flat plate. Hsu et al. [17] revealed the flow structure of oscillating channel flows and obtained $(Re_A)_{cr} = 2.00\times10^4$.

Recently, more studies are concentrated on heat transfer of oscillating pipe flows due to the increasing importance of the application in the ocean energy. Experimental studies show that the oscillating flows can enhance heat transfer. Experimental results of Chai *et al.* [18] show that the heat exchange capability of the oscillating heat pipe heat exchanger is about 3 times higher than that of a common tube heat exchanger. However their measurement is under the laminar flow region and they did not show the relationship of the enhancement of the heat transfer with governing parameters such as the Reynolds numbers. Wang and Lu [19] applied large eddy simulation (LES) technique to simulate heat transfer between the two constant temperature endplates of oscillating channel flow at Re = 350. They find out that the heat transfer takes place in a much thinner region near the wall at Pr = 100 than at Pr = 1. Due to the limitation of the computational speed of the LES method, they did not give out the full structures for heat transfer and fluid flow from laminar to transient and turbulent range. Also the assumption of the constant temperature difference between the two endplates does not fit for the present mode for sea water cooling heat exchangers, because the characteristic temperature difference is not on the pipe wall itself, but between inlet/outlet oscillating sea water and the pipe wall.

In the present study, the RANS method with Saffman's

Yan Su is with the Dept. of Electromechanical Engineering, Faculty of Science and Technology, University of Macau, Av. Padre Tomas Pereira, Taipa, Macau, China (phone: 853-8397-8466; fax: 853-2883-8314; e-mail: yansu@umac.mo).

Jane H. Davidson is with the Dept. of Mechanical Engineering, University of Minnesota, Minneapolis, MN 55455, USA (e-mail: jhd@me.umn.edu).

F. A. Kulacki is with the Dept. of Mechanical Engineering, University of Minnesota, Minneapolis, MN 55455, USA (e-mail: kulacki@me.umn.edu).

turbulence model was employed to study overall structures of the axis direction dominated flow and two dimensional heat transfer of oscillating flows in circular pipes. The experimental studies of [20] and [21] show that the entrance length of oscillating pipe flow can be approximated by $L_{entrance}/R = 8.76\times10^{-3}Re_R$. So the entrance length is a small value comparing to the transportation length of the water pipe before the water coming into the heat transfer part. Thus the flow can be assumed to be fully developed one dimensional dominated oscillating flow. Experimental study of a pulse combustor tail pipe in [22] showed that the mean temperature was as high as 800 K, while the surface temperature oscillated only about 0.56K. So the two dimensional heat transfer model with constant wall temperature Θ_w and inlet/outlet temperature Θ_0 boundary conditions is applied in the present study. Also the present model can speed up the simulation and make it possible for us to provide a complete picture of the oscillating flow structures and the overall heat transfer enhancement over a wide range of Re_A and Re_R. Results of oscillating velocity and temperature fields are decomposed by the method of partial sums of the Fourier series. The overall heat transfer enhancement comparing to a based line case of pure conduction will be presented. By the way of analyzing the overall Nusselt Number over wide ranges of the Reynolds number Re and Keulegan-Carpenter number *KC*, their effects on heat transfer and the potential application of the results in sea water cooling will also be discussed.

II. Governing Equations and Governing Parameters

Consider an oscillating flow in a pipe with radii *R*, the cylindrical coordinate is chosen such that *x* is in the flow direction parallel to the centerline of the pipe. The pressure gradient in the *x* direction that drives the flow is assumed to be cosinusoidal with a frequency *f* as:

$$-\frac{1}{\rho}\frac{\partial p}{\partial x} = \alpha_p \cos(2\pi f t) \tag{1}$$

where ρ is the fluid density, *p* the pressure, and α_p is the amplitude of negative pressure gradient which is assumed to be constant. Using α_p and *f*, a displacement length scale *A* is now defined as $A = \alpha_p/(2\pi f)^2$. Similarly as the oscillating channel flows discussed in [17], there are three length scales for oscillating flows in circular pipes: the displacement amplitude of fluid oscillation *A*, the pipe radius *R*, and the Stokes layer thickness δ. The Stokes layer thickness $\delta = \sqrt{\nu/2\pi f}$ measures the viscous diffusion distance in one cycle of oscillation, where, ν is the fluid viscosity and *f* is the oscillation frequency. The ratios of *A* and *R* to δ then give two important independent parameters defined respectively by $Re_A = A^2/\delta^2 = 2\pi f A^2/\nu$ and $Re_R = R^2/\delta^2 = 2\pi f R^2/\nu$. The oscillating period number, i.e. the Keulegan-Carpenter number *KC* (based on the characteristic length scale *R*) is defined as: $KC = 2\pi A/R = 2\pi(Re_A/Re_R)^{1/2}$, and the Reynolds number Re is defined as $Re = (2\pi f A)R/\nu = (Re_A Re_R)^{1/2}$.

Thus, in previous literatures we can see two set of governing parameters (Re_A, Re_R) and (*KC*, Re) for oscillating flow studies. The characteristics of the oscillating pipe flows then depend entirely on (Re_A, Re_R) or (*KC*, Re). While for heat transfer in oscillating pipe flows will also have Prantel number Pr as the third governing parameter. The coordinate systems for the two groups of governing parameters ($\log(Re_A)$, $\log(Re_R)$) and ($\log(KC)$, $\log(Re)$) differ $\pi/4$, so results can be presented in either of them.

Using *R* as the length scale, $2\pi f A$ as the velocity scale, $R/(2\pi f A)$ as the time scale, $\rho A(2\pi f)^2$ as the scale for negative pressure gradient, $\Theta_w - \Theta_0$ as the temperature scale, and the scales $(2\pi f A)^2$ and $2\pi f A/R$ for the pseudo-energy *e* and the pseudo-vorticity ω respectively, the non-dimensional governing equations can be obtained based on Saffman's turbulence model [13] as:

$$\frac{\partial u}{\partial t} = \frac{2\pi}{KC}\cos(2\pi t/KC) + \frac{1}{r}\frac{\partial}{\partial r}\left[r\left(\frac{1}{Re} + \gamma\frac{e}{\omega}\right)\frac{\partial u}{\partial r}\right] \tag{2}$$

$$\frac{\partial e}{\partial t} = \alpha_e e\left|\frac{\partial u}{\partial r}\right| - \beta_e e\omega + \frac{1}{r}\frac{\partial}{\partial r}\left[r\left(\frac{1}{Re} + \sigma_e\gamma\frac{e}{\omega}\right)\frac{\partial e}{\partial r}\right] \tag{3}$$

$$\frac{\partial \omega^2}{\partial t} = \alpha_\omega \omega^2\left|\frac{\partial u}{\partial r}\right| - \beta_\omega \omega^3 + \frac{1}{r}\frac{\partial}{\partial r}\left[r\left(\frac{1}{Re} + \sigma_\omega\gamma\frac{e}{\omega}\right)\frac{\partial \omega^2}{\partial r}\right] \tag{4}$$

$$\frac{\partial \Theta}{\partial t} + u\frac{\partial \Theta}{\partial x} = \frac{\partial}{\partial x}\left[\left(\frac{1}{Re\,Pr} + \gamma_T\frac{e}{\omega}\right)\frac{\partial \Theta}{\partial x}\right] + \frac{1}{r}\frac{\partial}{\partial r}\left[r\left(\frac{1}{Re\,Pr} + \gamma_T\frac{e}{\omega}\right)\frac{\partial \Theta}{\partial r}\right] \tag{5}$$

where, the Keulegan-Carpenter number $KC = 2\pi A/R$ is also the dimensionless period, and the Reynolds number $Re = (2\pi f A)R/\nu$, the $Pr = 7.0$ is selected to simulate water cooling in the present study.

The proper boundary conditions are:

$$u = 0,\ e = 0,\ \omega = \frac{S}{\alpha_e}\left|\frac{\partial u}{\partial r}\right|,\ \Theta = 1.0 \quad \text{at } r = \pm 1, \tag{6}$$

$$\frac{\partial u}{\partial r} = \frac{\partial e}{\partial r} = \frac{\partial \omega}{\partial r} = \frac{\partial \Theta}{\partial r} = 0 \quad \text{at } r = 0, \tag{7}$$

and

$$\Theta = 0 \qquad \text{at } x = \pm Lx/2R. \tag{8}$$

In (2)-(5), α_e, α_ω, β_e, β_ω, σ_e, σ_ω, γ and γ_T are universal constants. In the present computation, we followed Saffman & Wilcox [14] and Jacobs [23] to use $\alpha_e = 0.3$, $\alpha_\omega = 0.18$, $\beta_e = 0.09$, $\beta_\omega = 0.15$, $\sigma_e = 0.5$, $\sigma_\omega = 0.5$, $\gamma = 1.0$ and $\gamma_T = 1/0.89$. The value of *S* in the wall boundary condition (6) depends on the surface roughness and is equal to 100 for a smooth wall [14].

III. Numerical Procedure and Result Validation

A. Numerical Procedure

The equation system (2)-(5), subjected to boundary conditions (6)-(8), was solved numerically with the following procedures: (i) Central difference scheme for spatial derivatives, (ii) Second order Adams-Bashforth scheme for time advancement of the source terms, and (iii) Implicit scheme for the viscous terms.

The main reason for adapting Saffman's turbulence model rests on its applicability to flows over the entire range of Reynolds number to provide a first estimate of flow transition. Meanwhile, the simplicity of RANS method, especially the less time-consuming feature, enabled us to compute the flow and heat transfer characteristics over wide ranges of Reynolds numbers to provide a complete picture of the oscillating flow structure and the overall heat transfer enhancement.

In the present simulations, the length of the tube is 8 times of the diameter. A mesh with grid size 160×200 is used and the mesh is stretched by exponential function to provide more points near the wall and inlet/outlet of the pipe to resolve the Stokes layer near the tube wall and the entrance heat transfer. The dimensionless time step Δt was chosen as $\Delta t / KC = 10^{-6}$. The convergence error is less than 10^{-6} for the velocity field and less than 10^{-5} for the temperature field.

B. Validation by Comparing to Analytical Results of Laminar Oscillating Pipe Flows

When the Reynolds number Re_A is sufficiently low, the flow is laminar, i.e., $\langle u'w' \rangle = 0$ or $\gamma(e/\omega) = 0$. In term of the complex expression, $u = [\hat{u}\exp(i2\pi t/KC) + c.c]/2$ where $\hat{u}$ is the complex amplitude, $i = \sqrt{-1}$, and *c.c.* denotes the complex conjugate, the solution to (2) with boundary condition (6) and (7) is given by

$$\hat{u} = -i\left[1 - \frac{J_0\left(r\sqrt{-i\,\mathrm{Re}_R}\right)}{J_0\left(\sqrt{-i\,\mathrm{Re}_R}\right)}\right] \tag{9}$$

where, J_0 denotes the Bessel function of the first kind and of zero order. The amplitude and the phase angle of u are then obtained by taking the absolute value and the argument to $\hat{u}$, respectively.

The friction coefficient defined by $C_F = 2\tau_w/\rho(2\pi fA)^2 = [\hat{C}_F\exp(i2\pi t/KC) + c.c]/2$ with τ_w being the wall shear stress, can be obtained by taking the derivative to (9) with respect to r and evaluating the resultant equation at the wall to give the following expression:

$$\hat{C}_F = -\frac{2}{\mathrm{Re}}i\left[\frac{J_0'\left(r\sqrt{-i\,\mathrm{Re}_R}\right)\Big|_{r=1}}{J_0\left(\sqrt{-i\,\mathrm{Re}_R}\right)}\right] \tag{10}$$

Also, the amplitude and the phase angle of C_F are the absolute value and the argument of $\hat{C}_F$, respectively.

Two limit cases of high and low Re_R are of great interest. When $\mathrm{Re}_R \to \infty$, Eq. (9) reduces to

$$\hat{u} = -i\left\{1 - \frac{1}{r}\exp\left[-(1+i)\sqrt{\frac{\mathrm{Re}_R}{2}}(1-r)\right]\right\} \tag{11}$$

Equation (11) indicates that the oscillating velocity is composed of two Stokes layers near the walls (whose scale is of order δ) and the centerline velocity has an amplitude one and 90° phase-lag to the negative pressure gradient. By the same token, Eq. (10) reduces to

$$\hat{C}_F = (1-i)\frac{\sqrt{2\,\mathrm{Re}_R}}{\mathrm{Re}} = (1-i)\sqrt{\frac{2}{\mathrm{Re}_A}} \tag{12}$$

which indicates that the amplitude of wall shear stress depends solely on Re_A and has the phase angle 45° leading the centerline velocity. On the other hand, when $\mathrm{Re}_R \to 0$, Eq. (9) becomes the parabolic profile of a quasi-steady flow given by

$$\hat{u} = \left(1 - r^2\right)\mathrm{Re}_R/4 \tag{13}$$

which shows that the amplitude decreases with decreasing Re_R and the phase angle becomes in-phase with the negative pressure gradient. The wall shear stress of Eq. (10) now reduces to

$$\hat{C}_F = \mathrm{Re}_R/\mathrm{Re} = \left(\mathrm{Re}_R/\mathrm{Re}_A\right)^{1/2} \tag{14}$$

which shows that the amplitude of shear stress decreases with decreasing Re_R in 1/2 power if Re_A is fixed (i.e., when the amplitude of negative pressure gradient is fixed) and the phase angle is in-phase with the velocity (or negative pressure gradient).

To validate the present numerical code, computational results of the amplitudes and phase angles of centerline velocity u_C at $r = 0$ and wall shear stress C_F obtained by present code are compared with the analytical results from (9) and (10). As shown in Fig. 1, five cases for various Re_R ($<0.8\times10^4$) are in excellent agreement with those predicted from a laminar-flow analytic solution calculated from (9) and (10). From Fig. 1, we can see that when Re_R is larger than $10^{2.5}$ and less than 0.8×10^4, $|\hat{u}_C|$ equals to 1.0 and θ_{u_C} maintains constant at -90°. Similarly, $|\hat{C}_F|\mathrm{Re}_A^{1/2}$ is constant equal to 2.0 and θ_{C_F} remains constantly at -45°. These amplitudes and phase angles equal to those predicted by (11) and (12) for the limit case of $\mathrm{Re}_R \to \infty$. For laminar oscillating flows in two flat plate channels [17], as Re_R decreases, the amplitudes $|\hat{u}_C|$ and $|\hat{C}_F|\mathrm{Re}_A^{1/2}$ (shown in dashed lines in Fig. 1) overshoot to the maximum values greater than 1.0 and 2.0 respectively. For the present laminar oscillating flows in circular pipes, the amplitudes $|\hat{u}_C|$ overshoot to the maximum values greater than 1.0, however there is not overshooting for $|\hat{C}_F|\mathrm{Re}_A^{1/2}$. When Re_R becomes very low, the amplitudes of both u_C and C_F decrease and their phase angles approach zero. In fact, $|\hat{u}_C|$ varies linearly with Re_R and $|\hat{C}_F|\mathrm{Re}_A^{1/2}$ varies with $(\mathrm{Re}_R)^{1/2}$, which are agree with (13) and (14). The agreement of the numerical results and the analytical solution shown in Fig. 1, show that the present code works very well at low Re_R number range.

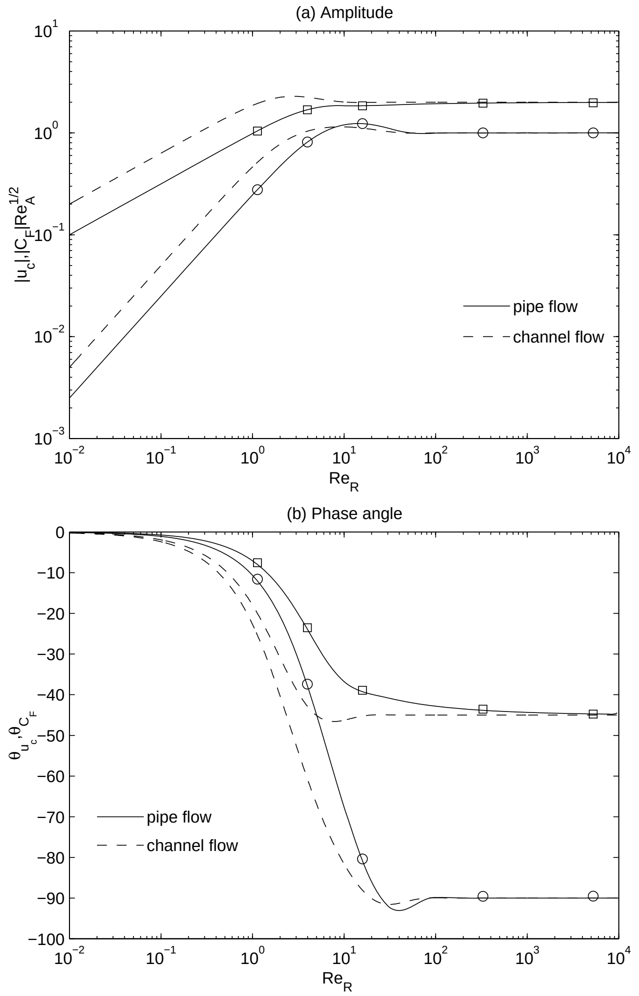

Fig. 1 Variations of centerline velocity u_C and wall frictional coefficient C_F with Re_R for oscillating laminar flow, (a) amplitude and (b) phase angle difference. Solid lines: analytical solution for laminar oscillating pipe flows from Eqs. (9) and (10); Dash lines: analytical solutions for laminar oscillating channel flows Hsu *et al* [17]; □- u_C and ○- C_F : computational results from present model

C. Validation by Comparing to Experimental Data of Turbulent Oscillating Pipe Flows

In order to validate the present code at high Reynolds number range, a comparison between our numerical result for one turbulent flow case (Re_R = 224.767 and $\mathrm{Re}_A = 6.2\times10^5$) and the experimental data of Akhavan (1991) has been done and shown in Fig. 2. The good agreement between the numerical results and experimental data on the transient velocity for the eight phase angles in a period guaranteed that the present code is also valid in high Reynolds number range.

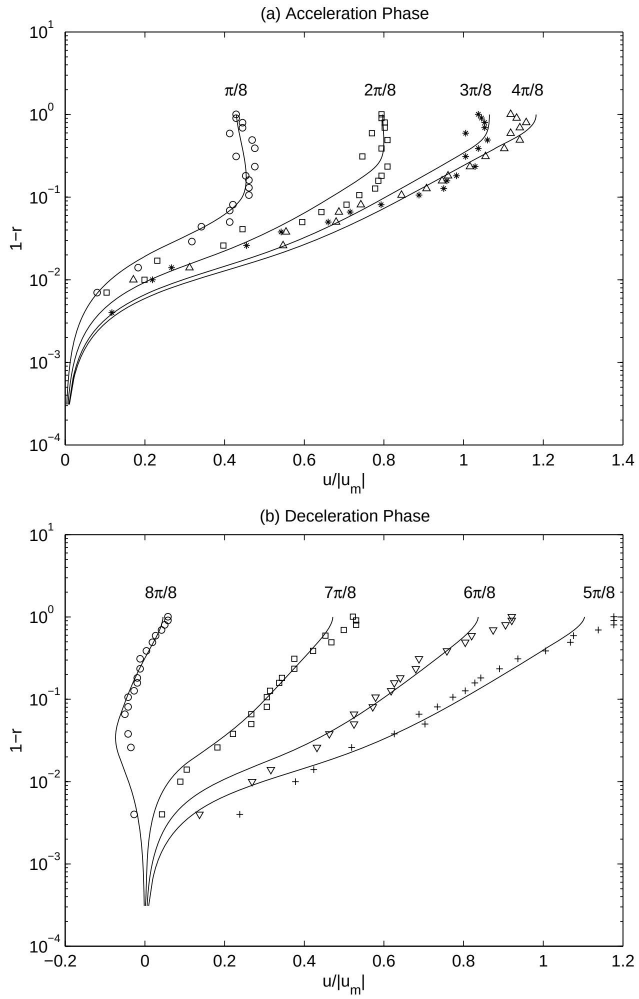

Fig. 2 A comparison between our numerical result and the experimental data of Akhavan [11]

IV. Result and Discussion

The method of partial sums of the Fourier series is used to decompose the velocity and temperature results. The velocity and temperature can be decomposed based on the dimensionless period of the oscillating pressure (i.e. the *KC* number) as:

$$u(r,t) = u_0(r) + \sum_{k=1}^{N} \hat{u}_k(r)\cos\left(k2\pi t / KC + \theta_k(r)\right) \tag{15}$$

and

$$\Theta(x,r,t) = \Theta_0(x,r) + \sum_{k=1}^{N} \hat{\Theta}_k(x,r)\cos\left(k2\pi t / KC + \theta_k(x,r)\right) \tag{16}$$

where, k is the order of the harmonic term and θ_k is phase angle difference comparing to the pressure phase angle. Zero order harmonic terms (u_0, Θ_0) are the cycle averaged values. The integer N larger than 3 is enough for decomposition of present numerical results, and higher orders of harmonic terms have maximum values of amplitude less than 10^{-5} and 10^{-3} for velocity and temperature field respectively, which are negligible.

A. Numerical Results for Fluid Flow

Numerical simulations for five different values of Re_R (= 5255, 328.4, 15.90, 3.974 and 1.131) and wide ranges of Re_A (from 10^3 to $10^{8.5}$) have been shown to cover the flow regimes from laminar to turbulent. It is noted that the present numerical simulation results contain in general the second and higher harmonics due to nonlinear nature in the equation system (2-4). Based on the decomposition of velocity as shown in (15), we find out that the fluid flow is dominated by the first order of harmonics.

A.1 Velocity Distribution along the r Direction

As our objective is to explore the flow structure for transition rather than non-linearity, only the amplitudes and the phase angles of the first order harmonic of the velocity results are presented in this paper.

To illustrate the flow transition under different conditions of Re_R, the velocity profiles of three different values of Re_A, corresponding to laminar, transitional and fully turbulent flows, are plotted in Fig. 3 for the two extreme cases of Re_R = 5255 (solid lines) and 3.974 (dashed lines). For the case of Re_R = 5255, Fig. 3 shows that the velocity profile at $\mathrm{Re}_A = 10^3$ is of a typical laminar oscillating flow with a thin Stokes layer near the wall and a potential core. When the flow becomes transitional at $\mathrm{Re}_A = 10^5$, the velocity profile shown in Fig. 3 indicates that the turbulent mixing is still confined in the turbulent boundary layer near the wall whose thickness is much thicker than the laminar Stokes layer. The locations of amplitude overshoot and phase-angle undershoot are shifted toward the pipe centerline due to turbulent mixing, even though the potential flow remains in the core region. At $\mathrm{Re}_A = 10^{8.5}$, the turbulent boundary layer apparently has occupied the whole pipe, the amplitude overshoot disappears. Alternatively, this can be interpreted as the location of overshoot has moved to the pipe centerline. The phase angle θ_u then becomes quite uniform across the pipe, but remains to be close to -90°. On the other hand, for the case of Re_R = 3.974 the velocity profile shown in Fig.3 indicates that the flow is laminar and nearly quasi-steady when $\mathrm{Re}_A = 10^3$, with an almost parabolic profile in $|\hat{u}|$ and phase angles θ_u ranging from -23.5° to -37.4°. When the flow becomes transitional at $\mathrm{Re}_A = 10^6$, the enhancement of the fluid diffusion by turbulent eddy viscosity apparently has flattened the velocity profile near the pipe core region to result in lower velocity amplitude. Meanwhile, the phase angle θ_u ranges from -18.1° to -21.8°, which indicates that the eddy viscosity effect renders the flow to approach toward the quasi-steady state. Further increase of the Reynolds number seems only to provide high eddy viscosity to further enhance the turbulent mixing effect toward a fully developed quasi-steady turbulent pipe flow, as shown by $\mathrm{Re}_A = 10^{8.5}$ in Fig. 3 and the phase angle θ_u ranges from -6.5° to -8.1°. The data also show that second order harmonic term of velocity is negligible comparing to the first order term and its phase angle is not as regular as that of the first hand harmonic term.

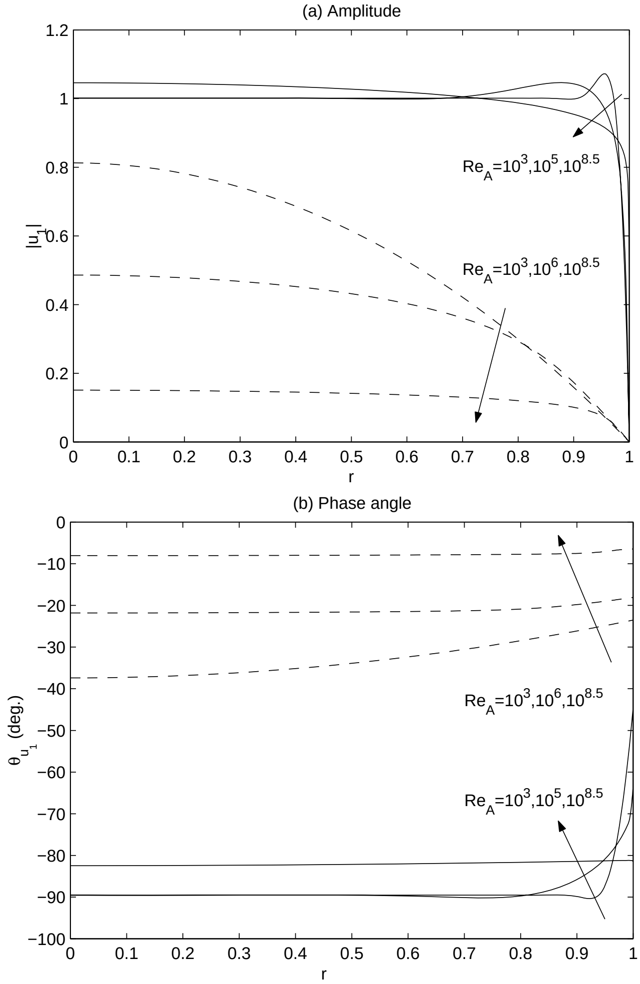

Fig. 3 First term of velocity profiles of laminar, transitional and turbulent oscillating flows for Re_R = 5255 (solid line) and Re_R =3.974 (dashed line), (a) amplitude of u_1, (b) phase angle of u_1

A.2 Full Structures of Velocity and the Wall Shear Stress

To obtain overall flow structures, the results of centerline velocity u_C and the wall shear stress C_F for all computed cases of Re_R and Re_A are plotted in Figs. 4 and 5, respectively, for (a) amplitude and (b) phase angle. In Figs. 4 and 5, the solid lines represent the analytical laminar flow results of low Re_A from Eq. (9) and (10) . We now first examine the result of u_C given in Fig. 4. For the two sets at high Reynolds numbers of Re_R = 5255 , the amplitudes $|\hat{u}_C|$ as shown in Fig. 4a maintain at one and the corresponding phase angles as shown in Fig. 4(b) have the value of -90°, except at very high Re_A. This suggests that the turbulent oscillating boundary layer for high Re_A is still thinner than R and is unable to produce noticeable effect on the centerline velocity, until Re_A becomes very high. For the cases of Re_R= 328.4, 15.90, 3.974 and 1.131, the values of $|\hat{u}_C|$ however drop monotonically with increasing Re_A in the turbulent regime. This is accompanied by the continuing shift of phase angle from -90° toward 0° as indicated in Fig. 4(b). Apparently, when Re_R is sufficiently small, the oscillating turbulent boundary layer becomes quasi-steady as $\mathrm{Re}_A \to \infty$. Assuming the flow is quasi-steady, the expression for $|\hat{u}_C|$ at very high Re_A can be devised by following Saffman's derivation [13] to give:

$$|\hat{u}_C| = \frac{1}{\kappa}\left(\frac{\mathrm{Re}_R}{\mathrm{Re}_A}\right)^{0.25}\left[0.25\ln(\mathrm{Re}_A) + 0.75\ln(\mathrm{Re}_R) + 1.92\right] \qquad (17)$$

where, κ ($0.38<\kappa<0.47$) is the von Kármán constant. The results calculated from (17) for high Re_A and low Re_R are shown as the dashed lines in Fig. 4a. They agree very well with the numerical results. It is recalled that in the quasi-steady limit where the shear layer covers the entire pipe, the pressure force is balanced totally by the shear. Therefore, we conclude that at very high Re_A, the eddy viscosity effect has greatly enhanced the shear force to render the transient inertia force negligible.

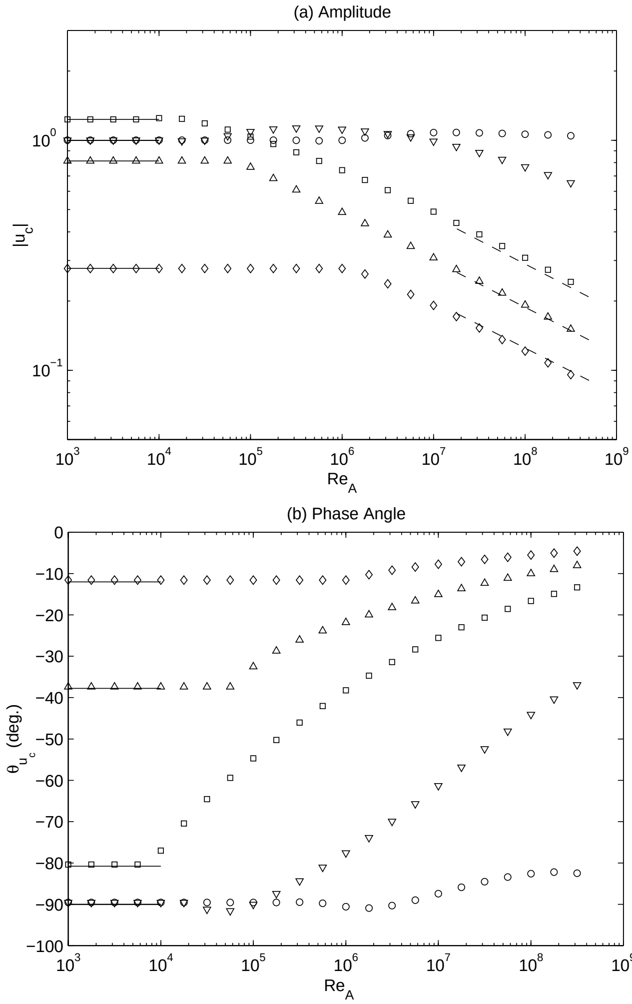

Fig. 4 Variations of (a) amplitude and (b) phase angle of u_C with Re_A for five values of Re_R. Solid lines: laminar solution; Dashed lines: quasi-steady analytical solution using Saffman's model [13]

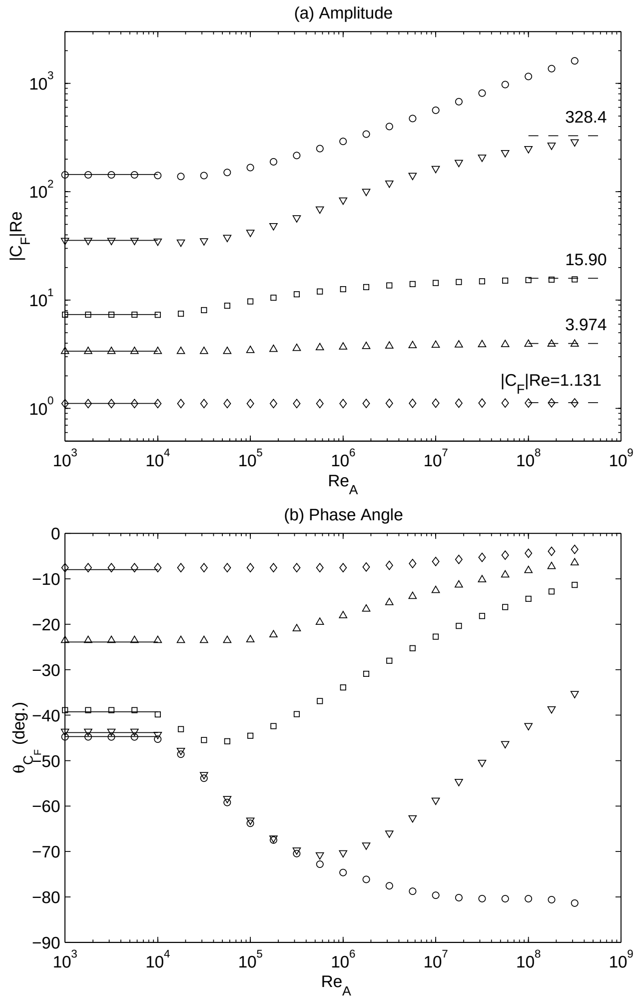

Fig. 5 Variations of (a) amplitude of C_F (b) phase angle of C_F with Re_A for five values of Re_R. Solid lines: laminar solution; Dashed lines: $|\hat{C}_F|\mathrm{Re} = \mathrm{Re}_R$.

For a better understanding of the flow structure, we shall examine the wall shear stress shown in Fig. 5. Attention is first given to the case of Re_R = 328.4, i.e, when R is about eighteen times the Stokes layer thickness δ. When Re_A is sufficiently low, say $\mathrm{Re}_A < 0.8\times10^4$ before flow transition, the oscillating flows are laminar. The results of C_F as computed according to the RANS method with Saffman's turbulence model agree excellently with the analytical predictions from (10), i.e., $|\hat{C}_F|\mathrm{Re}$ = 35.54 and θ_{C_F} = -43.84°. As Re_A increases, the transition from laminar to turbulent occurs approximately at $(\mathrm{Re}_A)_{cr} = 0.8\times10^4$ as shown in Fig. 5b where θ_{C_F} starts to decrease from -43.84°. Under the condition of Re_R = 328.4, the oscillating turbulent flow after transition remains as a boundary layer flow confined near the wall, with a potential flow in the pipe core region. Interestingly, the amplitude $|\hat{C}_F|\mathrm{Re}$ does not change noticeably until Re_A = 7.5×10^5, and hence is not a good indicator for flow transition. It is found out that the phase angle of the wall shear stress is a more sensitive gauge than amplitude for the determination of flow transition. Further increase in Re_A leads to higher value of the eddy viscosity ν_T that thickens the thickness δ_T of the oscillating turbulent boundary layer. The phase angle θ_{C_F} continues to decrease with increasing δ_T, until reaches a minimum value of about θ_{C_F} = -71° at $\mathrm{Re}_A = 7.5\times10^5$ where δ_T has become sufficiently thick that the effect due to the mutual interaction of the boundary layers at top and bottom of the channel is appreciable. For $\mathrm{Re}_A > 7.5\times10^5$, the phase angle θ_{C_F} increases with increasing Re_A. In the limit of $\mathrm{Re}_A \to \infty$, R becomes the governing length scale since $\delta_T >> R$ and the oscillating turbulent flow becomes a quasi-steady turbulent flow where $\theta_{C_F} \to 0$. The amplitude of wall shear stress given in Fig. 5a for Re_R = 328.4 shows that $\left|\hat{C}_F\right|\mathrm{Re}$ increases with increasing Re_A and asymptotically reaches a constant when $\mathrm{Re}_A \to \infty$. For a fully developed turbulent flow in a channel that is steady in mean and driven by a mean pressure gradient $\partial p/\partial x$, a simple momentum balance results in $\tau_w / R = -\partial p/\partial x$ which in terms of the friction coefficient becomes (14). This implies that Eq. (14), which was originally obtained for quasi-steady oscillating laminar flows, applies equal well to quasi-steady oscillating turbulent flows. The asymptotic value of $\left|\hat{C}_F\right|\mathrm{Re}$ is Re_R. This gives $\left|\hat{C}_F\right|\mathrm{Re}$ = 328.4 if Re_R = 328.4, which as shown as dashed line in Fig. 5a agrees very well with the computed result.

With the above comprehension of the flow for Re_R = 328.4, we now examine the flows at different Re_R. For higher Re_R such as the cases of Re_R = 5255, the oscillating laminar Stokes layer at low Re_A is much thinner than R. The transition from laminar to turbulent still occurs near $(\mathrm{Re}_A)_{cr} = 0.8\times10^4$; however, after the transition it requires much higher Re_A than that of Re_R = 328.4 for δ_T to become comparable with R. Fig. 5b indicates that θ_{C_F} reaches a minimum of -71° at $\mathrm{Re}_A = 7.5\times10^5$ for Re_R = 328.4 and is still decreasing at $\mathrm{Re}_A = 1.5\times10^7$ for Re_R = 5255. Figure 8a also shows that the amplitude results of this study never reach the asymptotic values of $\left|\hat{C}_F\right|\mathrm{Re}$ = 5255 for Re_R = 5255. Apparently, for the cases of Re_R = 5255 the computed range of Re_A in this study covers only the laminar Stokes layer flow and the oscillating turbulent boundary layer flow regimes. On the other hand, for the cases of low Re_R the thickness of the Stokes layer is already comparable with R when Re_R = 3.974 and much thicker than R when Re_R = 1.131. At low Re_A the flow is laminar with θ_{C_F} =-23.914° for Re_R = 3.974 and θ_{C_F} = -7.968° for Re_R = 1.131. The oscillating laminar flow is already in the quasi-steady flow regime. As Re_A increases passing the critical value $(\mathrm{Re}_A)_{cr}$, the oscillating flow moves directly from the quasi-steady laminar flow regime to the quasi-steady turbulent flow regime. Therefore, the phase angle θ_{C_F} increases from its respective laminar flow value toward 0°. Fig. 5a shows that for both cases of Re_R = 3.974 and 1.131 the amplitudes $\left|\hat{C}_F\right|\mathrm{Re}$ increases with increasing Re_A starting from $(\mathrm{Re}_A)_{cr}$ and reaches the asymptotic values of $\left|\hat{C}_F\right|\mathrm{Re}$ = 3.974 and 1.131, respectively, as plotted again as dashed lines. There is a delay in flow transition depending on Re_R. The lower the Re_R, the higher will be the $(\mathrm{Re}_A)_{cr}$ and the earlier the oscillating turbulent flow will reach the asymptotic results of quasi-steady state.

A.3 Flow Regimes

From the results given above, the structure of the oscillating pipe flows is constructed using parameters (Re_A, Re_R) as shown in Fig. 6. Each point on Fig. 6 represents one computed case. The open circle represents the laminar flow, the star represents the oscillating turbulent boundary layer flow and the triangle represents the quasi-steady turbulent flow. The transition from laminar regime to turbulent regime is marked by the sudden change of θ_{C_F} from the constant laminar values.

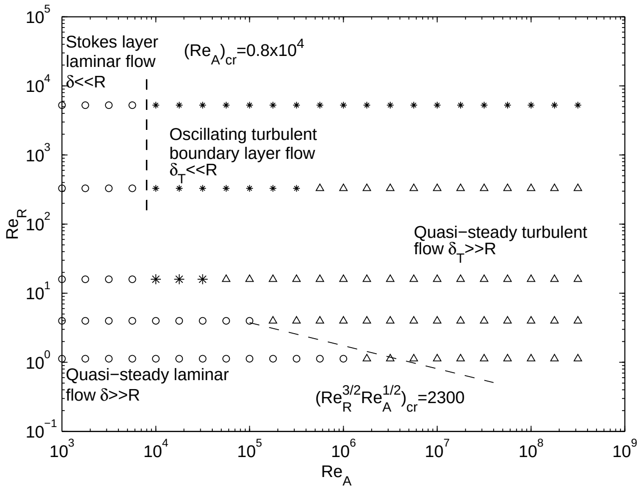

Fig. 6 Flow regimes of oscillating flows in channels in term of coordinates (Re_A , Re_R). ○: laminar flow; ▲: oscillating turbulent boundary layer flow; ▽: quasi-steady turbulent flow; Dashed lines: flow transition lines at the two extremes corresponding to boundary layer flows and quasi-steady viscous flows

At low Re_A , say $\mathrm{Re}_A < 0.8\times10^4$, the oscillating flows are laminar and two flow regimes showing low and high Re_R respectively, are identified. The domain of Re_R << 1 represents the quasi-steady laminar flow regime where the velocity profile is parabolic and the domain of Re_R >> 1 represents the Stokes layer laminar flow regime where the velocity profile decays exponentially from the wall. As Re_A increases, the Stokes layer at high Re_R becomes unstable. The transition from laminar to turbulent occurs approximately at $(\mathrm{Re}_A)_{cr} = 0.8\times10^4$ and is plotted as the dashed line in Fig. 6. For $\mathrm{Re}_A > (\mathrm{Re}_A)_{cr}$ and high Re_R , the flow is in the oscillating turbulent boundary layer flow regime where the thickness δ_T of turbulent boundary layer remains thinner than R, with a potential flow in the channel core. The increase in Re_A will lead to thicker δ_T and, in the limit of $\mathrm{Re}_A >> (\mathrm{Re}_A)_{cr}$ but still of high Re_R, the thickness δ_T becomes much thicker than R so that the flow is governed by R and belongs to the quasi-steady turbulent flow regime. The flow transition is delayed to higher $(\mathrm{Re}_A)_{cr}$ when Re_R decreases. In the limit of $\mathrm{Re}_R << 1$ where flows become quasi-steady, the transition is expected to occur at the same critical condition of a fully developed steady channel flow at $(\overline{U}2R/\nu)_{cr} = 2300$, where $\overline{U}$ is the mean velocity. For full developed pipe flow $\overline{U} = U_{\max}/2$. We have $U_{\max}=2\pi fA(\mathrm{Re}_R)/4$ from (13) and $(U_{\max}R/\nu)_{cr} = (\mathrm{ReRe}_R)_{cr}/4= 2300$; hence $(\mathrm{Re}_R^{3/2}\mathrm{Re}_A^{1/2})_{cr} = 9200$. This limit case of critical condition is also plotted in Fig. 6. Since the critical value of 9200 was found from experimental observation, which is less sensitive than our classification using phase angle change, the dashed line predicts a slightly higher value of $(\mathrm{Re}_A)_{cr}$. As Re_A passes $(\mathrm{Re}_A)_{cr}$, the oscillating flows move directly from the quasi-steady laminar flow regime into the quasi-steady turbulent flow regime.

B Numerical Results of Heat Transfer

Numerical results for the same five values of Re_R (= 5255, 328.4, 15.90, 3.974 and 1.131) and Re_A (from $10^{1.5}$ to $10^{7.5}$) have been presented to cover the heat transfer regimes from nearly conduction to laminar and turbulent flow convection. Also a pure conduction case is simulated as a base line for the study of heat transfer enhancement.

B.1 Temperature Distribution

It is noted that the present numerical simulation results for the temperature field contain higher orders of harmonics than the velocity field, because the fluid field will affect the temperature field as shown in (5). Based on the decomposition of the transient results of the temperature field, as shown in (16), we find out that the temperature field is dominated by the zero order of harmonic. The amplitude of the temperature harmonics will decrease with the increase of the order of harmonics. Phase angles are zero at the inlet/outlet of the pipe, while the phase angles at the center of the pipe (x=0) are the maximum value along the x direction. The phase angles will increase with the order of homogeneous, and the center phase angle is larger than 360 ^{o} at orders higher than the first order. For example, when Re_R = 1.131 and Re_A =100, the maximum amplitude of the zero order harmonic temperature is 1, and is about 0.4 for the first order. It is about 0.15 and 0.05 for the second and third harmonics respectively. The maximum phase angles appear in the mid of the tube at x=0. The maximum first order phase angle is about 120^{o} and it is about 390^{o} and 660 ^{o} for the second and the third order respectively. Our data also show that the thermal boundary layer thickness decreases with increase of Re_R or Re_A.Now that the amount of net heat transfer is based on the cycle averaged temperature gradient on the tube wall, so we will only discuss the Nusselt number based on the zero order of temperature gradient and the length scale R in the following parts to obtain the effects of parameters on net heat transfer.

B.2 Axis Direction Distribution of Nusselt Number

The axis direction distributions of the Nusselt Number on the pipe wall for Re_R = 328.4 and Re_A from 10^2 to $10^{7.5}$ are plotted as solid lines in Fig. 7. The dash line is the pure conduction result. With Re_A increased from 10^2 to $10^{7.5}$, the center point Nusselt number $Nu_R(x=0)$ will increase from 0 to 222. There is always a heat transfer leading edge near the inlet/outlet of the pipe due to the assumption of the constant inlet/outlet water temperature. The leading edge Nusselt numbers are much larger than the center ones. From Fig. 7, we can also see that the center point of Nusselt number equals 0 for the cases $\mathrm{Re}_A < 0.8\times10^4$, which is for nearly conduction to laminar flow regions. For the oscillating turbulent boundary layer flow region, when $\mathrm{Re}_A > 0.8\times10^4$, the center point Nusselt numbers will increase with Re_A.

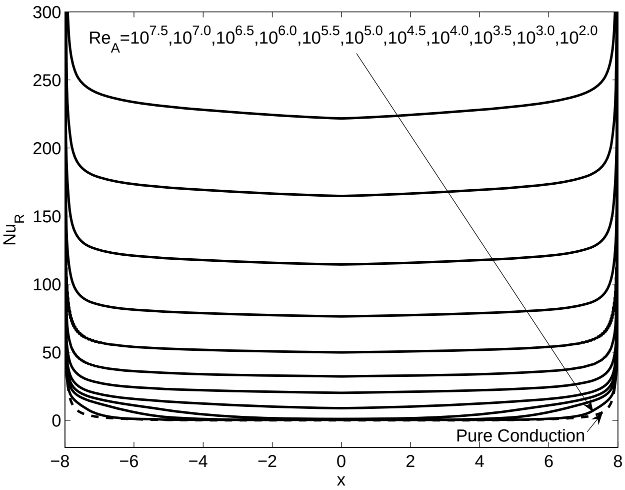

Fig. 7 Axis Direction Distribution of Nu_R on Wall (Dashed line: pure conduction, Solid lines: Re_R=328.4 and Re_A from 10^2 to $10^{7.5}$)

B.3 Averaged Nusselt Number based on various (Re_A, Re_R)

The averaged Nusselt Numbers along x direction are plotted in Fig.8 in form of Re_A and Re_R. At lower Re_A and Re_R, $\overline{Nu_R}$ is near to the pure conduction value (1.7031). While the value increase with both Re_A and Re_R. Those $\overline{Nu_R}$ lines in coordinate (Re_A, Re_R) never cross each other, which shows Re_R and Re_A are the basic two independent governing parameters for heat transfer as well as the structure of the flows in oscillating pipe flows. If $\overline{Nu_R}$ is plotted in form of Re and KC, we can see overlap of the data, which is similar as the overlap of data shown in the experimental study of [24].

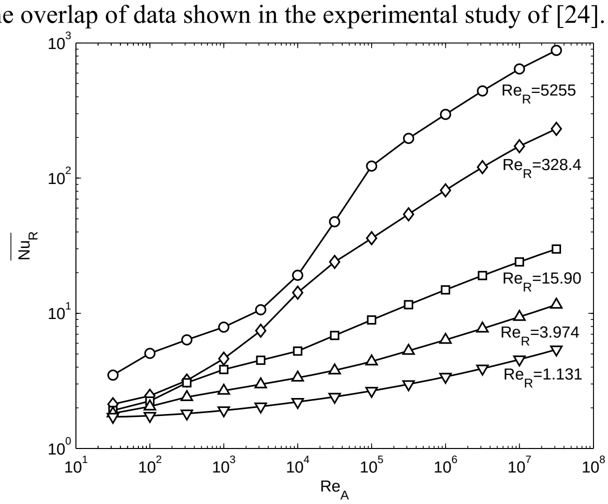

Fig. 8 Averaged Nusslet Number $\overline{Nu_R}$ for various cases

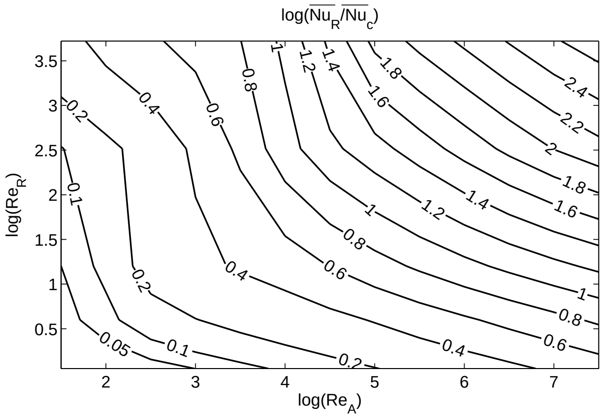

Fig. 9 Contour plot of log($\overline{Nu_R}$ / $\overline{Nu_C}$) in term of coordinates (log(Re_A), log(Re_R))

B.4 Heat Transfer Enhancement

Comparing to the pure conduction x axis averaged Nusselt Number ($\overline{Nu_C}$ =1.7031), the heat transfer enhancement ratio $\overline{Nu_R}$ / $\overline{Nu_C}$ is always greater than 1 in all ranges of Re_R and Re_A. Fig. 11 show the distribution of log($\overline{Nu_R}$ / $\overline{Nu_C}$) in term of coordinates (log(Re_A), log(Re_R)). From Fig. 11, we can see that the enhancement of heat transfer increased form near 1 at lower Re_A value less than 10^3 and lower Re_R value less than 4. The enhancement ratio is less than 10 for $\mathrm{Re}_A < 0.8\times10^4$ or $\mathrm{Re}_R < 10$. It means that in laminar flow and quasi-steady turbulent regions, the heat transfer enhancement is small and in order of 1. This similarity is consistent with the previous discussion on the quasi-steady turbulent flow has similar drag formation as laminar flow in (14). For oscillating turbulent boundary layer flow region, heat transfer enhancement ratio can be in order higher than 10. At higher Re_A and Re_R region such as Re_R =5255.0 and $\mathrm{Re}_A = 10^{7.5}$, the heat transfer enhancement ratio $\overline{Nu_R}$ / $\overline{Nu_C}$ can be as much as 500. From Fig. 9, we can see that increase of both Re_R and Re_A, i.e. increase of the pipe diameter R and the amplitude of the oscillating flow A, can definitely increase the heat transfer enhancement ratio. It is obviously that if we use larger pipe at places, where sea water oscillating amplitude as much as possible, we can get more effective heat transfer. Thus, we can remove thermal energy more quickly through sea water cooling by increase the oscillating amplitude and the pipe diameter. However the effect of the KC number on the heat transfer enhancement is not clear in Fig. 9, so in the following section, we will present a clear picture, which shows the effects of the KC numbers and Re numbers.

B.5 Optimal Keulegan-Carpenter number and Tube Diameter

In order to show the effects of the Keulegan–Carpenter number KC and the Reynolds number Re on the heat transfer, log($\overline{Nu_R}$) in form of coordinates (log(KC), log(Re)) is shown in Fig. 10. From Fig.10 we can see that log($\overline{Nu_R}$) increase dramatically with log(Re). Now that Re is linear to the velocity scale $2\pi fA$, we should put sea water cooling heat exchangers on sea floors, where both the frequency f and the amplitude A of the ocean wave are as large as possible. The circular white balls in Fig. 10 show the positions of the maximum $\overline{Nu_R}$ for a wide range of fixed Re number from 5 to 10^5. It is clear that $\overline{Nu_R}$ has a maximum value near the line of log(KC) ≈ 1.8, i.e. the optimal Keulegan–Carpenter number is about $10^{1.8}$ for heat transfer. Hence, in order to enhance the heat transfer between the tube wall and the sea water, the optimal KC number is about 63. Thus, the optimal size for the heat exchanger pipes should be around $R/A \approx 2\pi/10^{1.8}$, i.e. the inner diameter of the heat exchanger pipe over the wave oscillating amplitude should be $D/A \approx 4\pi/10^{1.8}$. So the optimal ratio of the inner diameter of the heat exchanger pipe over the ocean wave oscillating amplitude is $D/A \approx 0.2$.

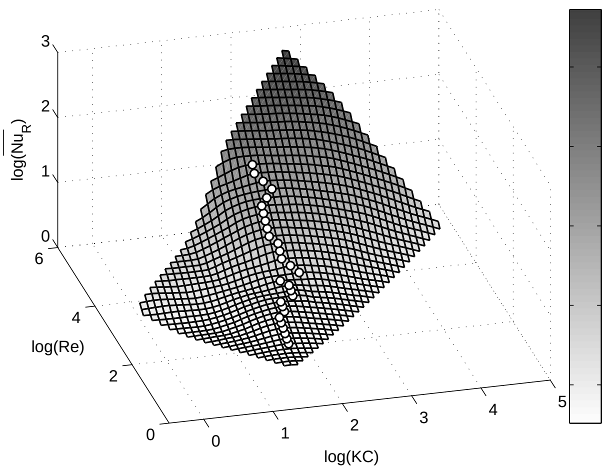

Fig. 10 Three dimensional plot of log($\overline{Nu_R}$) in term of coordinates (log(KC), log(Re)).

V. Conclusions

Fluid flow and heat transfer in oscillating pipe flows have been studied using RANS method with Saffman's turbulence model over wide ranges parameters to reveal the full structures of the fluid flow and heat transfer in oscillating pipe flows. For low Re_A, the flows are laminar and the present computed results are in excellent agreement with those predicted from a laminar-flow analytical solution. For laminar flow, the flow characteristics depend solely on Re_R, with $\mathrm{Re}_R >> 1$ corresponding to the Stokes layer flow limit and $\mathrm{Re}_R << 1$ to the quasi-steady laminar flow limit. As Re_A increases, the high Re_R Stokes layer flow becomes unstable at approximately $(\mathrm{Re}_A)_{cr} = 0.8\times10^4$ and experiences through a turbulent boundary layer flow regime before reaching a quasi-steady turbulent flow regime as $\mathrm{Re}_A \to \infty$, while the low Re_R quasi-steady laminar flow transits directly, with a delay, to the quasi-steady turbulent flow. This value of $(\mathrm{Re}_A)_{cr} = 0.8\times10^4$ agrees very well with the experimental results of Ohmi [10]. For turbulent oscillating flow, present numerical results (Re_R = 224.767 and $\mathrm{Re}_A = 6.2\times10^5$) and the experimental data of Akhavan [11] agree very well on both amplitude and phase angle. By the way of analyzing the overall Nusselt Number over wide ranges of the Reynolds number and Keulegan-Carpenter number, we know that $\overline{Nu_R}$ increase dramatically with the Re number and we also obtain the optimal *KC* number is about $10^{1.8}$ for a wide range of Re from 5 to 10^5. So the best place to put pipe heat exchangers for the application of sea water cooling is to choose the ocean floor, where both the frequency *f* and the amplitude *A* of the ocean water waves are as large as possible. The optimal ratio of the inner diameter of the heat exchanger pipe *D* over the wave oscillating amplitude *A* is $D/A \approx 0.2$.

ACKNOWLEDGMENT

The authors thank Prof. C. T. Hsu for his help on turbulent models. This study was supported by the Multi-Year Research Grant MYRG151(Y1-L2)-FST11-SY and the Start-Up Research Grant SRG009-FST11-YS of the Macau University. This study was also supported by the University of Minnesota Supercomputing Institute and the Information and Communication Technology Office of University of Macau.

REFERENCES

[1] Falcão, A.F.O. (2010). "Wave energy utilization: A review of the technologies." *Renewable and Sustainable Energy Reviews*, vol. 14, pp. 899–918.

[2] Harish, R., Subhramanyan, E.E., Madhavan, S. and Vidyanand, S. (2010). "Theoretical model for evaluation of variable frequency drive for cooling water pumps in sea water based once through condenser cooling water systems." *Applied Thermal Engineering*, vol. 30, pp. 2051-2057.

[3] Orazov, B., Savas, O., O'Reilly, O.M. (2010). "On the dynamics of a novel ocean wave energy converter" *Journal of Sound and Vibration*, vol. 329, n 24, pp. 5058-5069.

[4] Prudell, J., Stoddard, M., Amon, E., Brekken, T. K. A., Von Jouanne, A., (2010) "A permanent-magnet tubular linear generator for ocean wave energy conversion" *Transactions on Industry Applications*, vol. 46, no. 6, pp. 2392-2400.

[5] Sergeev, S. I. (1966). "Fluid oscillations in pipes at moderate Reynolds numbers" *Fluid Dynamics*, vol. 1, no. 1, pp. 121-122.

[6] Merkli, P. and Thomann, H. (1975). "Transition to turbulence in oscillating pipe flow" *Journal of Fluid Mechanics*, vol. 68, part 3, pp. 567-575.

[7] Hino, M., Sawamoto, M. and Takasu, S. (1976). "Experiments on transition to turbulence in an oscillatory pipe flow." *Journal of Fluid Mechanics*, vol. 75, part 2, pp. 193-207.

[8] Ohmi, M., Iguchi, M., Kakehachi, K. and Masuda, T. (1982). "Transition to turbulence and velocity distribution in an oscillating pipe flow," *Bulletin of the JSME*, vol. 25, no. 201, pp. 365-371.

[9] Ramaprian, B. R. and Tu, S. W. (1983). "Fully developed periodic turbulent pipe flow. Part 2. The detailed structure of the flow." *Journal of Fluid Mechanics*, vol. 137, pp. 59-81.

[10] Ohmi, M., Iguchi, M. and Akao, F. (1984). "Laminar-turbulent transition and velocity profiles of oscillatory rectangular duct flows." *Bulletin of the JSME*, vol. 27, no. 229, pp. 1399-1406.

[11] Akhavan, R., Kamm, R. D. and Shapiro, A. H. (1991). "An investigation of transition to turbulence in bounded oscillatory Stokes flows. Part 1. Experiments" *Journal of Fluid Mechanics*, vol. 225, pp. 395-422.

[12] Blondeaux, P. (1987). "Turbulent boundary layer at the bottom of gravity waves." *Journal of Hydraulic Research*, vol. 25, no. 4, pp. 447-464.

[13] Saffman, P. G. (1970). "A model for inhomogeneous turbulent flow" *Proceedings of the Royal Society of London*, Series A, vol. 317, pp. 417-433.

[14] Saffman, P. G. and Wilcox, P. C. (1974). "Turbulence-model predictions for turbulent boundary layers." *AIAA Journal*, vol. 12, no. 4, pp. 541-546.

[15] Koehler, W.J., Patankar, S.V. and Ibele, W. E., (1990) "Numerical prediction of turbulent oscillating flow in a circular pipe." *Proceedings of the Intersociety Energy Conversion Engineering Conference*, vol. 5, pp. 398-406.

[16] Hsu, C. T., Lu, X. and Kwan, M. K. (2000). "LES and RANS studies of oscillating flows over flat plate." *Journal of Engineering Mechanics*, vol. 126, no. 2, pp. 186-193.

[17] Hsu, C. T. and Kwan, M. K. (2001). "On the structure of oscillating channel flows" *Technical Report of Hong Kong University of Science and Technology*.

[18] Chai, B., Li, X., Zhou, S., Liu, D., Shao, M. and Peng, L. (2010). "Experimental study on energy saving of fluidized bed dryer with self-excited mode oscillating-flow heat pipe heat exchanger", *International Journal of Food Engineering*, vol. 6, no. 2, Article 5.

[19] Wang, L. and Lu, X. (2003). "An investigation of turbulent oscillatory heat transfer in channel flows by large eddy simulation." *International Journal of Heat and Mass Transfer*, vol. 47 pp. 2161–2172

[20] Yamanaka, G., Kikura, H., Takeda, Y. and Aritomi, M. (2002). "Flow measurement on an oscillating pipe flow near the entrance using the UVP method." *Experiments in Fluids*, vol.32, pp. 212-220.

[21] Gerrard, J. and Hughes, M. (1971). "The flow due to an oscillating piston in a cylindrical tube: a comparison between experiment and a simple entrance flow theory." *Journal of Fluid Mechanics*, vol. 50, pp. 97-106.

[22] Dec, J. E., Keller, J. O. and Arpaci, V. S., (1992) "Heat transfer enhancement in the oscillating turbulent flow of a pulse combustor tail pipe." *International Journal of Heat and Mass Transfer*, vol. 35, n 9, pp. 2311-2325.

[23] Jacobs, S. J. (1984). "Mass transport in a turbulent boundary layer under a progressive water wave." *Journal of Fluid Mechanics*, vol. 146, pp. 303-312.

[24] Rush, T.A., Newell, T.A., and Jacobi, A.M. (1999). "An experimental study of flow and heat transfer in sinusoidal wavy passages." *International Journal of Heat and Mass Transfer*, vol. 42, pp. 1541-1553.